Journal Name

RECEIVED
dd Month yyyy

REVISED
dd Month yyyy

PAPER Calculation of Tearing Mode Stability in a Magnetically Diverted Tokamak Plasma

Richard Fitzpatrick Institute for Fusion Studies, Department of Physics, University of Texas at Austin, Austin TX 78712, USA **E-mail:** rfitzp@utexas.edu

1 Introduction

All modern tokamak plasmas feature a *magnetic divertor*, which is a particular configuration of the magnetic field that redirects the outermost magnetic field-lines away from the confined plasma region, and into a controlled exhaust area, where the plasma particle and heat fluxes can safely be absorbed by a solid target plate [1]. Each magnetic flux-surface in a tokamak has an associated value of the *safety-factor*, which specifies the average number of toroidal circuits of the surface that a constituent magnetic field-line makes per poloidal circuit [2]. Magnetic flux-surfaces with rational values of the safety-factor are special. Indeed, non-axisymmetric tearing instabilities can drive magnetic reconnection on such *rational surfaces*, leading to localized changes in magnetic topology that degrade the ability of the surrounding flux-surfaces to confine energy. Alternatively, shielding currents can flow, predominately parallel to magnetic field-lines, on rational surfaces, and act to suppress magnetic reconnection [3].

A magnetically diverted tokamak plasma possesses a so-called "last closed magnetic flux-surface" (LCFS). Magnetic flux-surfaces that lies inside the LCFS are topologically simple tori, and are completely occupied by plasma. Magnetic flux-surfaces that lies outside the LCFS have more complicated topology, and are only partly occupied by plasma. The LCFS features a magnetic "X-point", which is a circular loop, coaxial with the plasma torus, on which the poloidal magnetic field is zero. (In some very special tokamak plasmas, the LCFS features two X-points. However, we shall not consider such plasmas here.) As the LCFS is approached, the safety-factor exhibits a logarithmic singularity [4], as a direct consequence of the presence of the X-point, and there is an associated accumulation of rational flux-surfaces around the LCFS. In fact, for an tearing instability with a given toroidal mode number, there are, in principle, an infinite number of associated rational surfaces, most of which lie close to the LCFS, on which the mode can drive magnetic reconnection. Practically speaking, it is impossible to include all of these surfaces in a stability calculation. Hence, it is common practice to simply ignore rational flux-surfaces associated with very high values of the safety-factor. The aim of this paper is to investigate to what extent this procedure is justified.

2 Two-Filament Model of a Magnetically Diverted Plasma

2.1 Introduction

The aim of this section is to construct a very simple model of a magnetically diverted tokamak plasma.

2.2 Equilibrium Magnetic Field

Suppose that two current filaments run parallel to the z-axis [4]. Let the first filament carry the current I_p, and pierce the x-y plane at $x = y = 0$. Let the second filament carry the current I_c, and pierce the x-y plane at $x = 0$, $y = -a$. The first filament represents the "toroidal" (i.e., z-directed) plasma current, whereas the second represents the toroidal current flowing in the magnetic divertor coil. Suppose that there is a uniform, externally generated, toroidal magnetic field of strength B_0. Let the system be periodic in the z direction with period $2\pi\, R_0$, where R_0 is the simulated major radius of the plasma. It is helpful to define the simulated toroidal angle, $\phi = z/R_0$.

The equilibrium magnetic field can be written in the divergence-free manner

$$\mathbf{B} = \nabla\phi \times \nabla\psi_p + B_0\, R_0\, \nabla\phi, \tag{1}$$

where

$$\psi_p(x,y) = \frac{\mu_0\, I_p\, R_0}{4\pi}\, \ln\left(x^2 + y^2\right) + \frac{\mu_0\, I_c\, R_0}{4\pi}\, \ln\left[x^2 + (y+a)^2\right] \tag{2}$$

is the "poloidal" (i.e., circulating in the x-y plane) magnetic flux (divided by 2π) generated by the two current filaments.

2.3 Flux Coordinates

It is convenient to re-express the magnetic field in the usual Clebsch form

$$\mathbf{B} = \nabla(\phi - q\,\theta) \times \nabla\psi_p, \tag{3}$$

where θ is a poloidal angle, and $q = q(\psi_p)$ the (dimensionless) *safety-factor* [5]. Equations (1) and (3) can be reconciled provided

$$\nabla\psi_p \times \nabla\theta \cdot \nabla\phi = \frac{B_0}{R_0\, q}. \tag{4}$$

Note, from Eq. (3), that $\mathbf{B} \cdot \nabla\psi_p = 0$, which implies that ψ_p is a magnetic flux-surface label. Furthermore, $\mathbf{B} \cdot \nabla(\phi - q\,\theta) = 0$, which implies that magnetic field-lines within a given flux-surface appear as straight lines, with gradient $d\phi/d\theta = q$, when plotted in the θ-ϕ plane. In fact, ψ_p, θ, ϕ are known as *flux-coordinates*, and θ is termed a *straight* poloidal angle [5].

2.4 Non-Diverted Edge Safety-Factor

In the absence of the divertor current, the plasma would have a circular cross-section of minor radius a, and an edge safety-factor value of

$$q_* = \frac{2\pi\, B_0\, a^2}{\mu_0\, I_p\, R_0}. \tag{5}$$

2.5 Normalization Scheme

Let $x = a\,X$, $y = a\,Y$, $\nabla = a^{-1}\,\hat{\nabla}$, and $\psi_p = \mu_0\, I_p\, R_0\, \psi/(2\pi)$. It follows that

$$\hat{\nabla}\psi \times \hat{\nabla}\theta \cdot \hat{\nabla}\phi = \frac{a}{R_0}\,\frac{q_*}{q}, \tag{6}$$

$$\psi = \frac{1}{2}\,\ln\left(X^2 + Y^2\right) + \frac{\beta}{2}\,\ln\left[X^2 + (Y+1)^2\right], \tag{7}$$

$$\psi_X = \frac{X}{X^2 + Y^2} + \frac{\beta\, X}{X^2 + (Y+1)^2}, \tag{8}$$

$$\psi_Y = \frac{Y}{X^2 + Y^2} + \frac{\beta\,(Y+1)}{X^2 + (Y+1)^2}, \tag{9}$$

where $\beta = I_c/I_p$. Here, $\psi_X \equiv \partial\psi/\partial X$, et cetera.

2.6 Magnetic X-point

The magnetic X-point is located at the point in the X-Y plane where $\psi_X = \psi_Y = 0$ (i.e., where the poloidal magnetic field-strength is zero). As is easily demonstrated, the coordinates of this point are (X_c, Y_c), where $X_c = 0$ and $Y_c = -1/(1+\beta)$. The magnetic separatrix corresponds to the curve $\psi(X, Y) = \psi_c$, where

$$\psi_c \equiv \psi(X_c, Y_c) = \ln\left[\frac{\beta^{\,\beta}}{(1+\beta)^{1+\beta}}\right]. \tag{10}$$

It is helpful to define the normalized poloidal flux $\Psi = \psi_c/\psi$. (Note that this definition is different from the conventional one, $\Psi = \psi/\psi_c$, because $\psi \to \infty$ on the magnetic axis, $X = Y = 0$, and we wish the normalized flux to increase as we go from the axis to the separatrix.)

2.7 Construction of Flux Coordinate System

Equation (6) yields

$$\frac{d\theta}{dL} = \frac{q_*}{q\,|\hat{\nabla}\psi|}. \tag{11}$$

where dL is an element of normalized length around a magnetic flux-surface. It follows that

$$q(\psi) = \frac{q_*}{2\pi} \oint \frac{dL}{|\hat{\nabla}\psi|}, \tag{12}$$

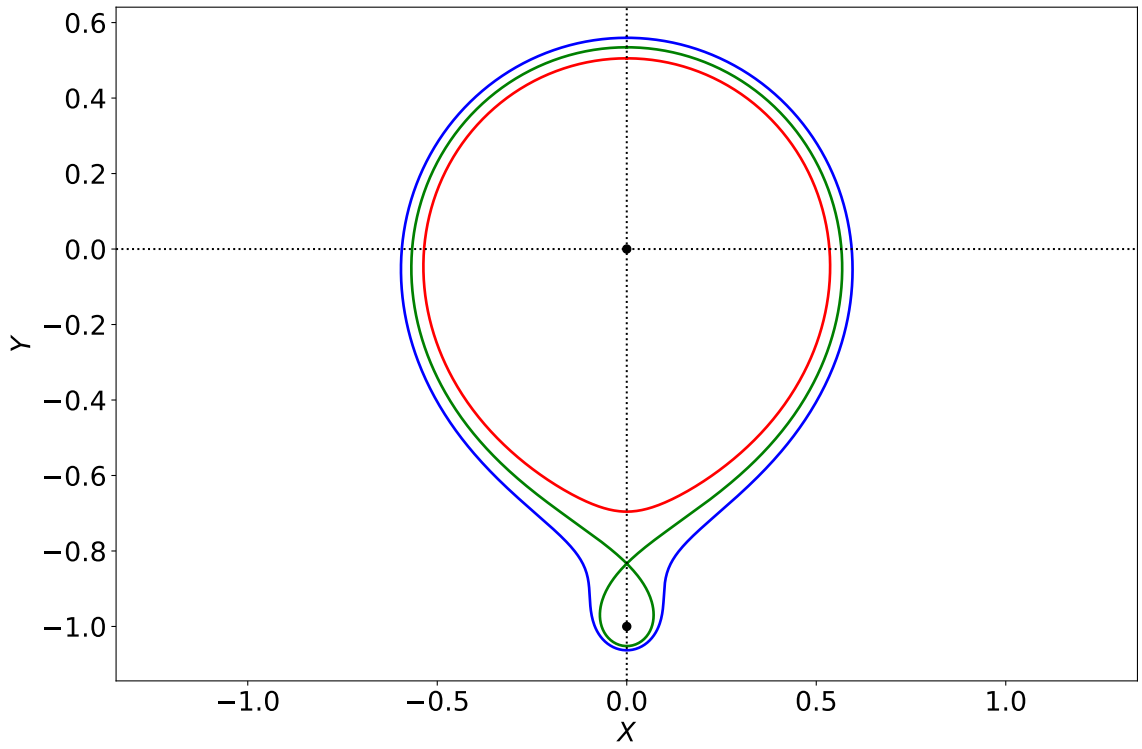

Figure 1. The magnetic flux-surfaces $\Psi = 0.9$ (red), $\Psi = 1.0$ (green), and $\Psi = 1.1$ (blue) in the absence of a divertor plate. The black dots shows the locations of the two current filaments. Here, $q_* = 12$ and $\beta = 0.2$.

where $\oint$ implies a complete circuit in θ at constant ψ. It is easily demonstrated that, on such a circuit,

$$\frac{dX}{dL} = -\frac{\psi_Y}{\sqrt{\psi_X^2 + \psi_Y^2}}, \tag{13}$$

$$\frac{dY}{dL} = \frac{\psi_X}{\sqrt{\psi_X^2 + \psi_Y^2}}, \tag{14}$$

$$\frac{d\phi}{dL} = \frac{q_*}{\sqrt{\psi_X^2 + \psi_Y^2}}, \tag{15}$$

$$\frac{d\varpi}{dL} = \frac{X\,\psi_X + Y\,\psi_Y}{(X^2+Y^2)\sqrt{\psi_X^2 + \psi_Y^2}}, \tag{16}$$

where

$$\varpi = \tan^{-1}\left(\frac{Y}{X}\right) \tag{17}$$

is a geometric poloidal angle. Here, ϕ is calculated on the assumption that we are following a magnetic field-line within the flux-surface (i.e., $d\phi/d\theta = q$). We need to integrate Eqs. (13)–(16) from $\varpi = 0$ to $\varpi = 2\pi$, subject to the initial condition $\phi(\varpi = 0) = 0$, and then set $q(\psi) = \phi(\varpi = 2\pi)/(2\pi)$. We can then compute θ using

$$\frac{d\theta}{dL} = \frac{q_*}{q\sqrt{\psi_X^2 + \psi_Y^2}}. \tag{18}$$

Let $q_* = 12$ and $\beta = 0.2$. Figure 1 shows the magnetic flux-surfaces $\Psi = 0.9$, $\Psi = 1.0$, and $\Psi = 1.1$, plotted in the X-Y plane. Flux-surfaces characterized by $\Psi < 1$ do not enclose the divertor current filament, whereas those characterized by $\Psi < 1$ do enclose the filament. The magnetic separatrix, $\Psi = 1$, separates flux-surfaces that do and do not enclose the divertor current filament, and crosses itself at the magnetic X-point.

The red and blue curves in Fig. 2 show the safety-factor profile, $q(\Psi)$, inside and outside the magnetic separatrix, respectively. It is clear that the safety-factor generally increases with increasing Ψ. However, $q \to \infty$ as $\Psi \to 1$. In other words, the safety-factor tends to infinity as the

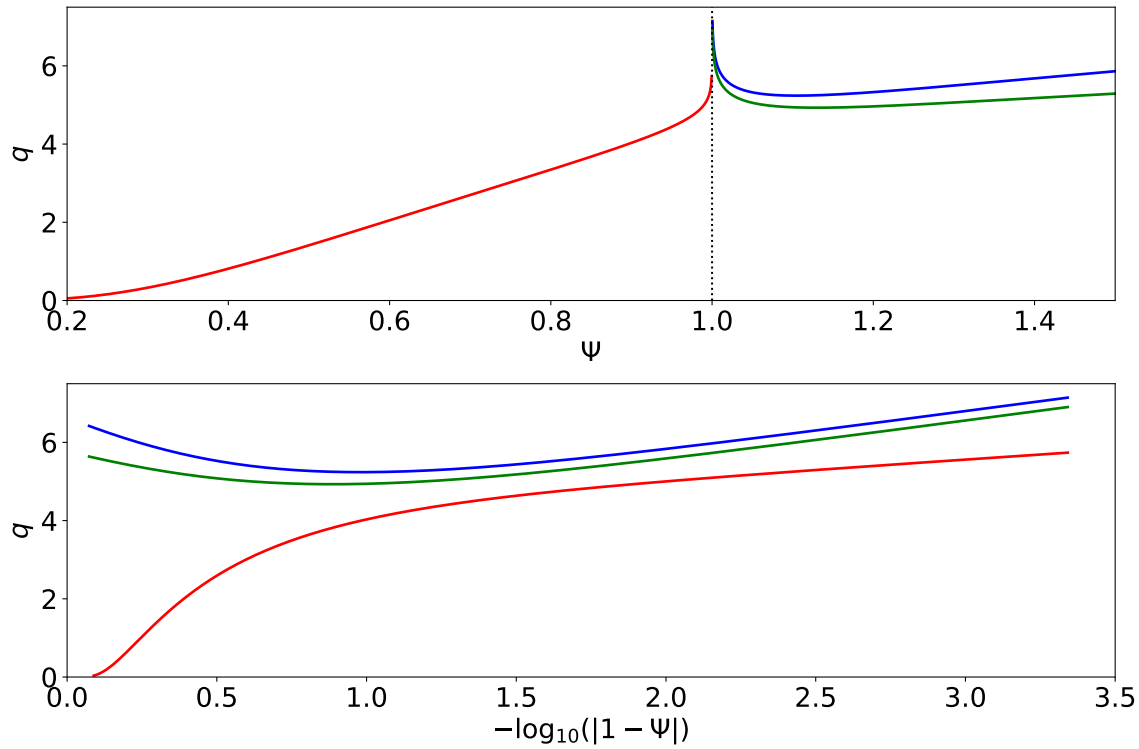

Figure 2. The safety-factor profile, $q(\Psi)$. The red curve shows the safety-factor inside the magnetic separatrix. The blue and green curves show the safety-factor outside the separatrix in the absence and in the presence of a divertor plate, respectively. Here, $q_* = 12$ and $\beta = 0.2$

magnetic separatrix is approached from either direction. It is apparent from the bottom panel of Fig. 2 that q approaches infinity *logarithmically* as $\Psi \rightarrow 1$ (because the plot of q versus $\log_{10}(|\Psi - 1|)$ asymptotes to a straight line as $|\Psi - 1| \rightarrow 0$). In other words, close to the separatrix, we can write

$$q(\Psi) \simeq -\alpha_- \, \log(1 - \Psi) \tag{19}$$

for $\Psi < 1$, and

$$q(\Psi) \simeq -\alpha_+ \, \log(\Psi - 1) \tag{20}$$

for $\Psi > 1$. Moreover, it is clear from the figure that $\alpha_+ > \alpha_-$.

Figures 3 and 4 show the flux coordinate system inside and outside the magnetic separatrix, respectively. It can be seen that, as the magnetic separatrix is crossed, all of the contours of θ converge onto, and then diverge away from, the X-point. This singular behavior occurs because the Jacobian of the flux coordinate system, $\mathcal{J} \equiv (\hat{\nabla}\psi \times \hat{\nabla}\theta \cdot \hat{\nabla}\phi)^{-1} = (R_0/a)\,(q/q_*)$, is infinite at the X-point.

2.8 Significance of Flux Coordinates

To understand the significance of the flux coordinate system, suppose that the plasma is subject to a magnetic perturbation that varies with θ, ϕ, and time, t, as $\exp[\mathrm{i}\,(m\,\theta - n\,\phi - \omega\,t)]$. Here, m and n are integers. In other words, the perturbation (which is, of course, single-valued in the angular coordinates θ and ϕ) possesses m periods in the poloidal angle, n periods in the toroidal angle, and rotates at the (complex) angular frequency ω. The curl of the perturbed, linearized, electron fluid equation of motion yields

$$[\omega + n\,(\omega_E + \omega_{*\,e})]\left[b^{\psi_p} - \frac{B_0}{R_0\,q}\,(m - n\,q)\,\xi^{\psi_p}\right] \simeq \frac{B_0}{R_0\,q}\,m\,\eta_\parallel\,j_\phi, \tag{21}$$

where subscripts and superscripts denote covariant and contravariant components in the ψ_p, θ, ϕ coordinate system, respectively. Here, $\mathbf{b}$ is the perturbed magnetic field, $\boldsymbol{\xi}$ the Largrangian electron fluid displacement, $\mathbf{j}$ the perturbed current density, and $\eta_\parallel$ the plasma parallel electrical resistivity. Moreover,

$$\omega_E(\psi_p) = -\frac{d\Phi}{d\psi_p} \tag{22}$$

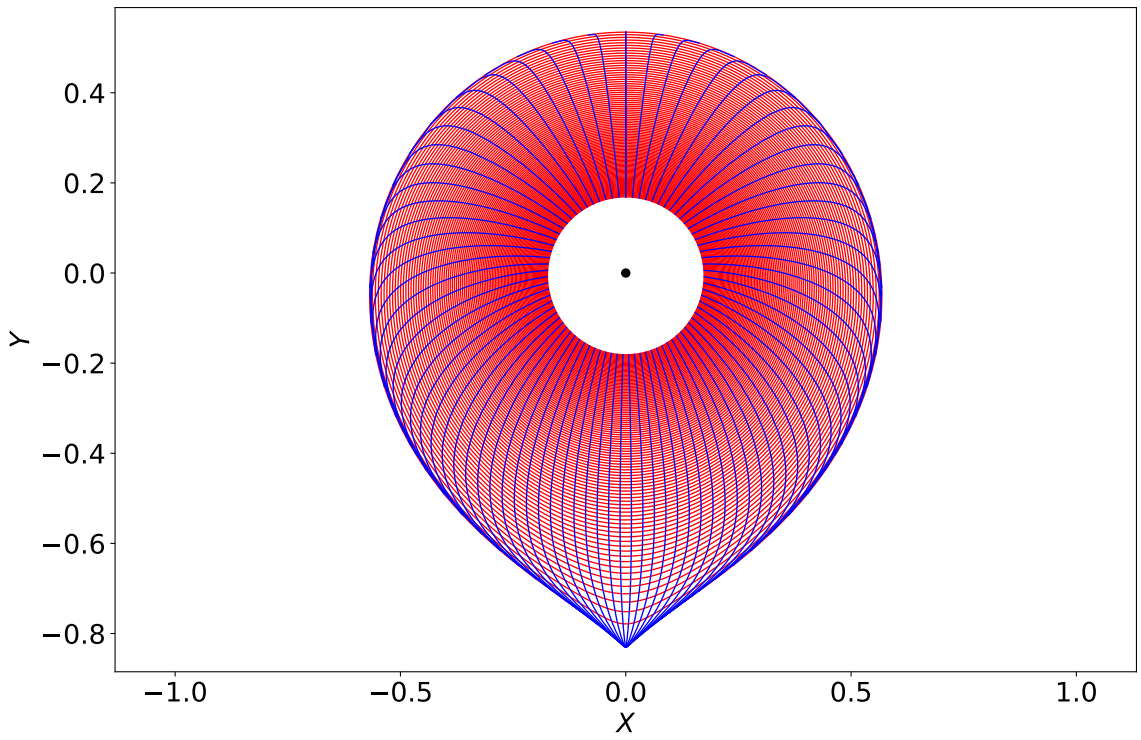

Figure 3. The flux coordinate system inside the magnetic separatrix. The red curves are surfaces of constant $\hat{\psi}$, whereas the blue curves are surfaces of constant θ. The black dot shows the location of the plasma current filament. Here, $q_* = 12$ and $\beta = 0.2$

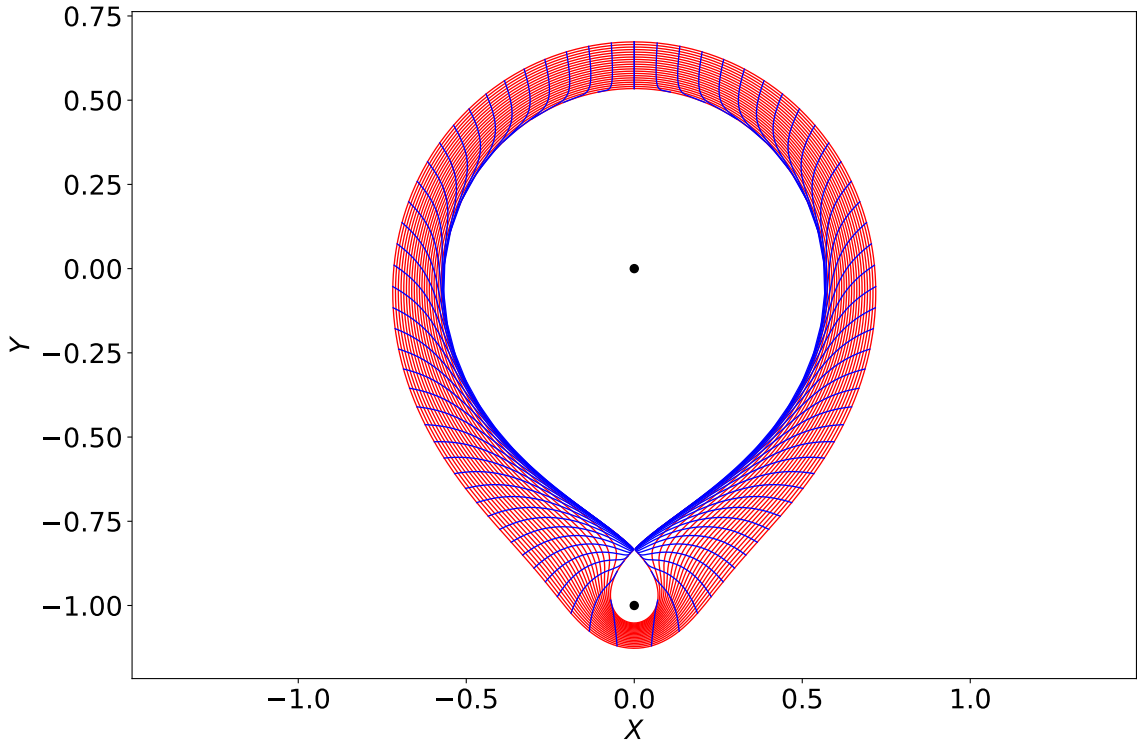

Figure 4. The flux coordinate system outside the magnetic separatrix in the absence of a divertor plate. The red curves are surfaces of constant $\hat{\psi}$, whereas the blue curves are surfaces of constant θ. The black dots shows the locations of the two current filaments. Here, $q_* = 12$ and $\beta = 0.2$.

is the *E-cross-B frequency*, whereas

$$\omega_{*\,e}(\psi_p) = \frac{1}{e\,n_e}\,\frac{dp_e}{d\psi_p} \tag{23}$$

is the *electron diamagnetic frequency*. Here, $\Phi(\psi_p)$ is the electrostatic potential, $p_e(\psi_p)$ the electron pressure, $n_e(\psi_p)$ the electron number density, and e the magnitude of the electron charge.

Equation (21) describes how the inductive electric field generated by a time-varying magnetic field, as seen in rest frame of the local electron fluid, attempts to drive a current parallel to magnetic field-lines. On a general magnetic flux-surface, the two terms (in the large square brackets) on the left-hand side of the equation cancel one another out, and there is no driven current. In other words, the electron fluid displaces rather than allowing a parallel inductive current to flow. However, it is clear from the equation that there exist a special magnetic flux-surface, termed a *rational* flux-surface, at which the safety-factor takes the rational value $q = m/n$ [5]. On the rational flux-surface, the two terms on the left-hand side of Eq. (21) cannot cancel one another out, because the second term is zero everywhere on the surface. Hence, in general, a parallel inductive current is driven on the rational flux-surface. The current is a *shielding current* that acts to suppress magnetic reconnection on the flux-surface, or, at least, to slow down reconnection such that it takes place on the comparatively long resistive timescale [3, 6].

We can now appreciate that, by employing a flux coordinate system, we can distinguish rational magnetic flux-surfaces from irrational flux-surfaces. (A rational surface is one on which the associated safety-factor can be expressed as a rational number. Note that this definition only makes sense if the safety-factor is a flux-surface function.) We can also determine the angular variation of the particular magnetic perturbation that drives a shielding current on a particular rational surface. Note, finally, that Figs. 2–4 make it clear that rational flux-surfaces exist both inside and outside the magnetic separatrix.

2.9 Effect of Divertor Plate

The reason that rational magnetic flux-surfaces exist outside the magnetic separatrix is because the flux-surfaces in this region form closed loops, that complete below the divertor filament, when plotted in the X-Y plane. In fact, this must be the case in an axisymmetric system otherwise the divergence of the magnetic field would be non-zero. Thus, the commonly used term "last closed magnetic flux-surface" (meaning the magnetic separatrix) is inaccurate. All of the magnetic flux-surfaces are closed. However, those outside the magnetic sepatatrix are only partly occupied by plasma because they intersect the divertor plate.

Suppose that the divertor plate is horizontal (i.e., parallel to the X-axis), and is situated halfway between the X-point and the divertor filament. When integrating Eqs. (13)–(16), we are really integrating along the path of a shielding current filament excited by an inductive electric field. Under normal circumstances, the filament is constrained to run parallel to magnetic field-lines. However, within the divertor plate, the filament takes the path of least electrical resistance, which implies that it runs along the X-axis at constant ϕ. It follows that, within the divertor plate, Eqs. (13)–(16) must be replaced by

$$\frac{dX}{dL} = 1, \tag{24}$$

$$\frac{dY}{dL} = 0, \tag{25}$$

$$\frac{d\phi}{dL} = 0, \tag{26}$$

$$\frac{d\varpi}{dL} = -\frac{Y}{X^2+Y^2}. \tag{27}$$

Again, let $q_* = 12$ and $\beta = 0.2$. Figure 5 shows the magnetic flux-surfaces $\Psi = 0.9$, $\Psi = 1.0$, and $\Psi = 1.1$, plotted in the X-Y plane. Note that the surfaces $\Psi = 1.0$ and $\Psi = 1.1$ both have sections that run parallel to the divertor plate. Strictly speaking, these sections are not magnetic flux-surfaces (the actual magnetic flux-surfaces complete below the divertor plate, as shown in Fig. 1), but instead represent the paths of shielding current filaments.

The green curve in Fig. 2 shows the safety-factor profile calculated outside the magnetic separatrix in the presence of the divertor plate. Note that the safety-factor is decreased in the presence of the plate, because shielding current filaments can take a short-cuts through it, rather than having to run in loops below it.

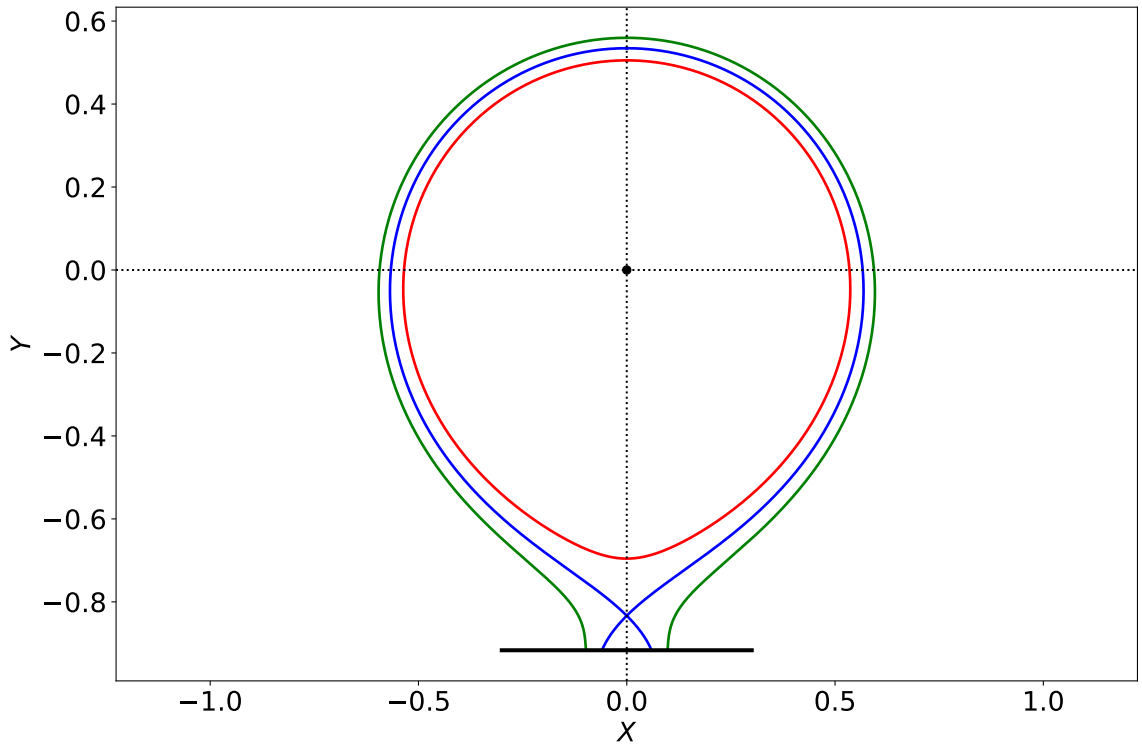

Figure 5. The magnetic flux-surfaces $\Psi = 0.9$ (red), $\Psi = 1.0$ (green), and $\Psi = 1.1$ (blue) in the presence of a divertor plate located halfway between the X-point and the divertor filament. The black dot shows the location of plasma current filament, and the horizontal black line shows the location of the divertor plate. Here, $q_* = 12$ amd $\beta = 0.2$.

Finally, Fig. 6 shows the flux coordinate system outside the magnetic separatrix in the presence of the divertor plate. Observe that the divertor plate is a surface of constant θ.

2.10 Summary

In this section, we have constructed a very simple model of a magnetically diverted plasma. We find that it is possible to construct a flux coordinate system both inside and outside the magnetic separatrix, even in the presence of a divertor plate. We can also define a safety-factor profile outside the separatrix. This implies that rational magnetic "flux-surfaces" (with sections that run along the divertor plate) exist outside the separatrix, and that we can determine the angular variation of the magnetic perturbations that would excite shielding currents on these surfaces.

3 Improved Model of a Magnetically Diverted Plasma

3.1 Introduction

The model described in Sect. 2 has the unrealistic feature that $q = 0$ at the magnetic axis. This feature is an artifact of treating the plasma current as a filament, rather than a spatially extended distribution. In this section, we shall attempt to construct an improved model.

3.2 Equilibrium Magnetic Field

Let R, ϕ, Z be conventional cylindrical coordinates that are coaxial with the plasma torus. We can express the equilibrium magnetic field in the divergence-free manner [6]

$$\mathbf{B} = \nabla\phi \times \nabla\psi_p + B_0\, R_0\, g\, \nabla\phi = \nabla(\phi - q\,\theta) \times \nabla\psi_p. \tag{28}$$

Here, ϕ is a true toroidal angle, ψ_p the true poloidal magnetic flux (divided by 2π), $g(\psi_p)$ an arbitrary (dimensionless) flux-function, $q(\psi_p)$ the safety-factor, R_0 the major radius of the magnetic axis, and B_0 the vacuum toroidal magnetic field-strength on the axis (which implies that $g = 1$ in the vacuum region surrounding the plasma). The previous equation is only self-consistent if

$$\nabla\psi_p \times \nabla\theta \cdot \nabla\phi = \frac{B_0\, R_0\, g}{R^2\, q}. \tag{29}$$

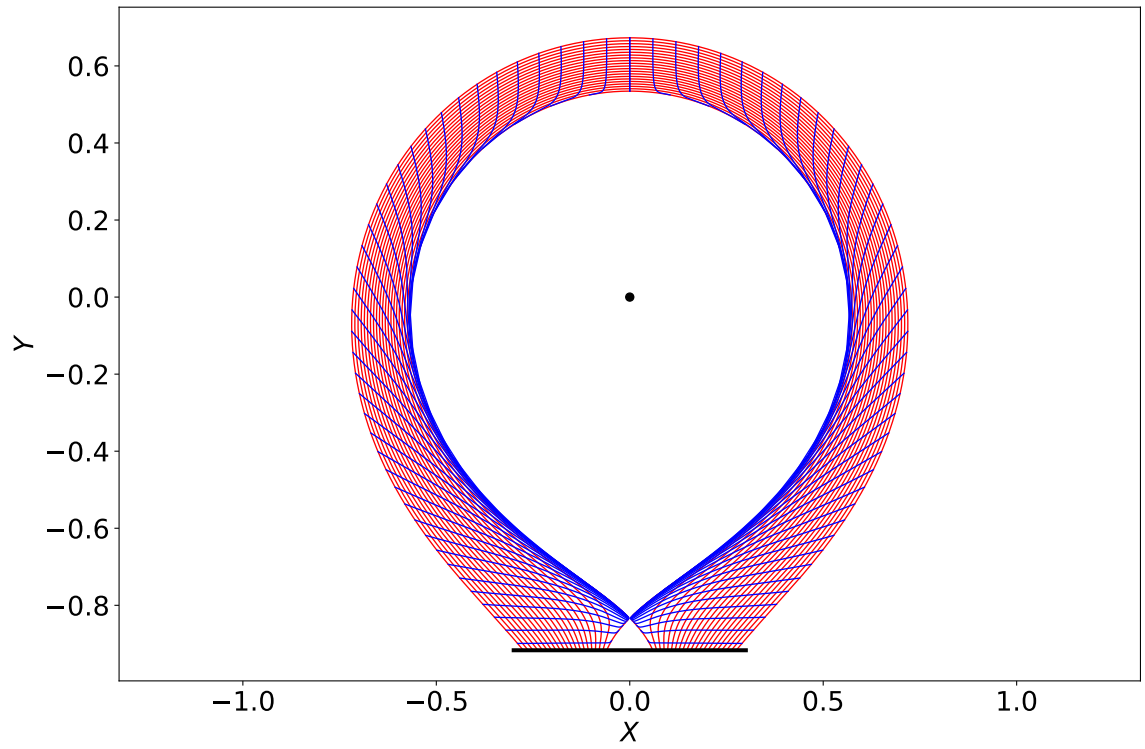

Figure 6. The flux coordinate system outside the magnetic separatrix in the presence of a divertor plate located halfway between the X-point and the divertor filament. The red curves are surfaces of constant $\hat{\psi}$, whereas the blue curves are surfaces of constant θ. The black dot shows the location of the plasma filament, and the horizontal black line shows the location of the divertor plate. Here, $q_* = 12$ and $\beta = 0.2$.

It is helpful to define a magnetic flux-surface label, r, with the dimensions of length, as follows [6]:

$$\frac{d\psi_p}{dr} = \frac{B_0\, r\, g}{q}. \tag{30}$$

It is easily demonstrated that

$$\nabla r \times \nabla\theta \cdot \nabla\phi = \frac{R_0}{R^2\, r}. \tag{31}$$

Here, r can be interpreted as the mean minor radius of a given magnetic flux-surface. Suppose that the magnetic separatrix corresponds to the flux-surface $r = a$. Thus, we can interpret a as the mean minor radius of the plasma. Moreover, flux-surfaces with $r < a$ lie inside the separatrix, whereas those with $r > a$ lie outside.

3.3 Model Safety-Factor Profile

Let us adopt a model safety-factor profile inspired by the analysis of Sect. 2. Let $\hat{r} = r/a$. Suppose that

$$q(\hat{r}) = q_0 - \alpha_-\, \ln\left(1 - \hat{r}^{\,2}\right) \tag{32}$$

for $\hat{r} < 1$, and

$$q(\hat{r}) = -\alpha_+\, \ln\left(\hat{r}^{\,2} - 1\right) \tag{33}$$

for $\hat{r} > 1$, where

$$\alpha_- = -\frac{q_{95} - q_0}{\ln(1 - \hat{r}_{95}^2)}, \tag{34}$$

$$\alpha_+ = -\frac{q_{105}}{\ln(\hat{r}_{105}^2 - 1)}. \tag{35}$$

Here, q_0 is the safety-factor on the magnetic axis ($\hat{r} = 0$), q_{95} is the safety-factor on the magnetic flux-surface that encloses 95% of the poloidal magnetic flux enclosed by the magnetic separatrix,

$\hat{r}_{95}$ is the $\hat{r}$-coordinate of the 95% flux-surface, q_{105} is the safety-factor on the magnetic flux-surface that encloses 105% of the poloidal magnetic flux enclosed by the magnetic separatrix, and $\hat{r}_{105}$ is the $\hat{r}$-coordinate of the 105% flux-surface.

3.4 Poloidal Magnetic Flux

We wish to determine the poloidal flux in the vicinity of the magnetic separatrix. Let $\psi_p = B_0\, a^2\, \psi$. It follows from Eq. (30) that

$$\frac{d\psi}{d\hat{r}} \simeq \frac{\hat{r}}{q}, \tag{36}$$

assuming that we can set $g \simeq 1$ close to the separatrix.

For $\hat{r} < 1$, Eqs. (32) and (36) yield

$$\frac{d\psi}{d\hat{r}} = \frac{\hat{r}}{q_0 - \alpha_-\, \ln(1-\hat{r}^{\,2})}, \tag{37}$$

which can be integrated to give

$$\psi(\hat{r}) = \frac{\mathrm{e}^{\,q_0/\alpha_-}}{2\,\alpha_-}\left\{E_1\left(\frac{q_0}{\alpha_-}\right) - E_1\left[\frac{q_0}{\alpha_-} - \ln\left(1-\hat{r}^{\,2}\right)\right]\right\}, \tag{38}$$

where $E_1(x)$ is an exponential integral [7]. Hence,

$$\psi(1) = \frac{\mathrm{e}^{\,q_0/\alpha_-}}{2\,\alpha_-}\, E_1\left(\frac{q_0}{\alpha_-}\right) \tag{39}$$

is the normalized poloidal flux enclosed within the magnetic separatrix. Let $\Psi(\hat{r}) = \psi(\hat{r})/\psi(1)$. It follows that

$$\Psi(\hat{r}) = 1 - \frac{E_1[q_0/\alpha_- - \ln(1-\hat{r}^{\,2})]}{E_1(q_0/\alpha_-)} = 1 - \frac{E_1(q/\alpha_-)}{E_1(q_0/\alpha_-)}. \tag{40}$$

By definition, $\Psi(\hat{r}_{95}) = 0.95$, so

$$\frac{E_1(q_{95}/\alpha_-)}{E_1(q_0/\alpha_-)} = 0.05. \tag{41}$$

Assuming that q_0 and q_{95} are specified, the previous equation can be solved to give α_-, which then allows $\hat{r}_{95}$ to be determined from Eq. (34).

For $\hat{r} > 1$, Eqs. (33) and (36) yield

$$\frac{d\psi}{d\hat{r}} = -\frac{\hat{r}}{\alpha_+\, \ln(\hat{r}^{\,2}-1)}, \tag{42}$$

which can be integrated to give

$$\psi(\hat{r}) = \psi(1) + \frac{E_1[-\ln(\hat{r}^{\,2}-1)]}{2\,\alpha_+}. \tag{43}$$

Thus,

$$\Psi(\hat{r}) = 1 + \frac{\alpha_-}{\alpha_+}\,\mathrm{e}^{-q_0/\alpha_-}\,\frac{E_1[-\ln(\hat{r}^{\,2}-1)]}{E_1(q_0/\alpha_-)} = 1 + \frac{\alpha_-}{\alpha_+}\,\mathrm{e}^{-q_0/\alpha_-}\,\frac{E_1(q/\alpha_+)}{E_1(q_0/\alpha_-)}, \tag{44}$$

where use has been made of Eq. (39). By definition, $\Psi(\hat{r}_{105}) = 1.05$. Hence, Eqs. (41) and (44) can be combined to give

$$\frac{E_1(q_{105}/\alpha_+)}{\alpha_+} = \mathrm{e}^{\,q_0/\alpha_-}\,\frac{E_1(q_{95}/\alpha_-)}{\alpha_-}. \tag{45}$$

Assuming that q_{105} is specified, the previous equation can be solved to give α_+, which then allows $\hat{r}_{105}$ to be determined from Eq. (35).

Consider a plasma equilibrium characterized by $q_0 = 1.01$, $q_{95} = 3.5$, and $q_{105} = 4.0$. We can solve Eqs. (41) and (45) to give $\alpha_- = 1.196$ and $\alpha_+ = 2.163$. Equations (34) and (35) then reveal that $\hat{r}_{95} = 0.9355$ and $\hat{r}_{105} = 1.076$. The resulting model safety-factor profile in the vicinity of the magnetic separatrix is shown in Fig. 7.

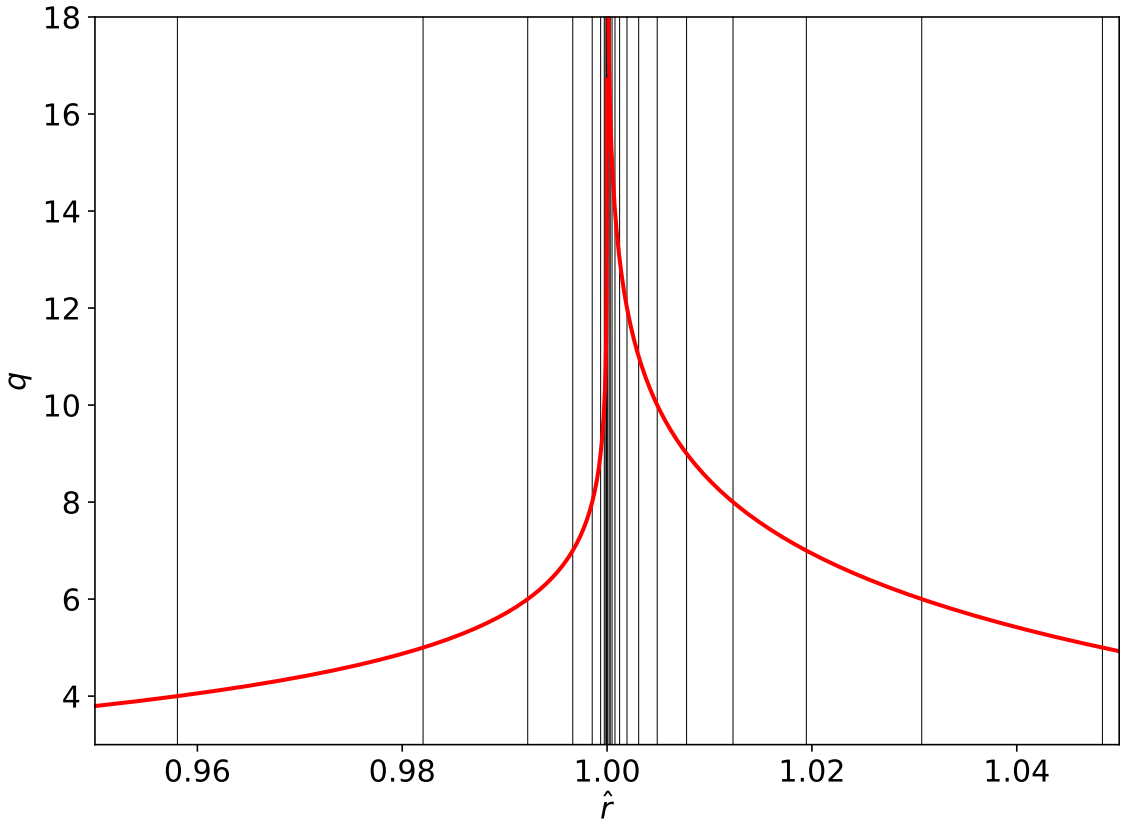

Figure 7. The model safety-factor profile in the vicinity of the magnetic separatrix, calculated for $q_0 = 1.01$, $q_{95} = 3.5$, and $q_{105} = 4.0$. The black vertical lines show the locations of the $n = 1$ rational surfaces.

4 Tearing Stability

4.1 Introduction

The aim of this section is to formulate the tearing stability problem in the presence of a magnetic separatrix.

4.2 Ideal-MHD Perturbation

Suppose that the plasma equilibrium is subject to a tearing perturbation that possesses n periods in the toroidal direction, and is such that [8]

$$\frac{r\, b^r(r,\theta,\phi,t)}{B_0\, R_0} = \mathrm{i}\left(\frac{R_0}{R}\right)^2 \sum_m \psi_m(r)\, \mathrm{e}^{\,\mathrm{i}\,(m\,\theta - n\,\phi + \omega\, t)}, \tag{46}$$

where $b^r = \mathbf{b}\cdot\nabla r$, $\mathbf{b}$ is the perturbed magnetic field, and the ψ_m are dimensionless. Note that the perturbation consists of a single toroidal harmonic, but multiple coupled poloidal harmonics characterized by the set of integer poloidal mode numbers m. Everywhere in the plasma, apart from the immediate vicinity of the various rational surfaces, the tearing mode is governed by the perturbed, linearized equations of ideal-MHD [9]. These equations reduce to a set of coupled ordinary differential equations (o.d.e.s) that take the form [6, 8]

$$r\,\frac{d\psi_m}{dr} = \sum_{m'} \frac{L_m^{m'}\, Z_{m'} + M_m^{m'}\, \psi_{m'}}{m' - n\,q}, \tag{47}$$

$$(m - n\,q)\, r\,\frac{d}{dr}\left(\frac{Z_m}{m - n\,q}\right) = \sum_{m'} \frac{N_m^{m'}\, Z_{m'} + P_m^{m'}\, \psi_{m'}}{m' - n\,q}. \tag{48}$$

Here, the (dimensionless) $Z_m(r)$ are related to the perturbed toroidal magnetic field. Moreover, the (dimensionless) $L_m^{m'}(r)$, $M_m^{m'}(r)$, $N_m^{m'}(r)$, and $P_m^{m'}(r)$ coefficients are functions of the equilibrium profiles and the metric elements of the r, θ, ϕ coordinate system [8]. Note that Eqs. (47) and (48) are singular at rational magnetic flux-surfaces at which $q = m/n$.

The locations of the $n = 1$ rational surfaces for our model safety-factor profile are indicated in Fig. 7. It can be seen that rational surfaces accumulate in the vicinity of the magnetic separatrix, where $q(\hat{r})$ has a logarithmic singularity. Moreover, rational surfaces exist both inside and outside the separatrix.

The accumulation of rational surfaces at the magnetic separatrix is problematic. In principle, for a given toroidal mode number, there are an infinite number of rational surfaces, the majority of which lie very close to the separatrix. It would be be prohibitively difficult to include all of these surfaces in a tearing stability calculation. Let us investigate whether this is really necessary.

4.3 Behavior in Vicinity of Rational Surface

Consider the solution of the ideal-MHD o.d.e.s, (47) and (48), in the vicinity of a rational surface, of radius r_s, where $q(r_s) = m/n$, and m is the resonant poloidal mode number. Let $x = r - r_s$. At small values of $|x|$, the function $\psi_m(r)$ takes the form [6, 8]

$$\psi_m(r_s + x) = A_L^{\pm}\,|x|^{\,\nu_L}(1 + \lambda_L\,x) + A_S^{\pm}\,\mathrm{sgn}(x)\,|x|^{\,\nu_S} + A_C\,x + \mathcal{O}(x^2), \tag{49}$$

where

$$\nu_L = \frac{1}{2} - \sqrt{-D_I}, \tag{50}$$

$$\nu_S = \frac{1}{2} + \sqrt{-D_I}, \tag{51}$$

$$D_I = -L_0\,P_0 - \frac{1}{4}, \tag{52}$$

$$L_0 = -\left(\frac{L_m^m}{m\,s}\right)_{r_s}, \tag{53}$$

$$P_0 = -\left(\frac{P_m^m}{m\,s}\right)_{r_s}, \tag{54}$$

$$s = \frac{d\ln q}{d\ln r}, \tag{55}$$

and λ_L and A_C are defined in Refs. [6] and [8]. The superscripts $+$ and $-$ correspond to $x > 0$ and $x < 0$, respectively. Here, $A_L^{\pm}$ are known as the *coefficients of the large solution*, whereas $A_S^{\pm}$ are termed the *coefficients of the small solution*. The *Mercier interchange stability parameter*, D_I, is assumed to be negative. (Otherwise, the the rational surface would be unstable to localized ideal interchange modes [10].) Note that ν_L and ν_S are known as *Mercier indices*.

For the case of a tearing mode, the coefficients of the large solution to the left and the right of a rational surface have to be equal to one another. In other words, $A_L^+ = A_L^- = A_L$. Note, however, that the coefficients of the small solution to the left and the right of a rational surface are not, in general, equal to one another.

4.4 Tearing Mode Dispersion Relation

Let us index the various rational surfaces in the plasma by means of an integer k. Note that this is possible even if there are an infinite number of such surfaces. Thus, the kth rational surface possesses the minor radius r_k, the resonant poloidal mode number m_k, the coefficient of the large solution $A_{L\,k}$, the coefficients of the small solution $A_{S\,k}^{\pm}$, and the Mercier indices $\nu_{L\,k}$ and $\nu_{S\,k}$. It is helpful to define the quantities [6, 8]

$$\Psi_k = r_k^{\,\nu_{L\,k}}\left(\frac{\nu_{S\,k} - \nu_{L\,k}}{L_{m_k}^{m_k}}\right)_{r_k}^{1/2} A_{L\,k}, \tag{56}$$

$$\Delta\Psi_k = r_k^{\,\nu_{S\,k}}\left(\frac{\nu_{S\,k} - \nu_{L\,k}}{L_{m_k}^{m_k}}\right)_{r_k}^{1/2} (A_{S\,k}^{+} - A_{S\,k}^{-}). \tag{57}$$

at each rational surface. Here, the complex dimensionless parameter Ψ_k is a measure of the reconnected magnetic flux at the kth rational surface, whereas the complex dimensionless parameter $\Delta\Psi_k$ is a measure of the strength of the radially localized shielding current that flows around the surface.

The general tearing mode dispersion relation takes the form [6, 8]

$$\Delta\Psi_k = \sum_{k'} E_{kk'}\,\Psi_{k'}, \tag{58}$$

and specifies the shielding current that is excited in the vicinity of the kth rational surface in response to reconnected magnetic flux at the other rational surfaces. Here, $E_{kk'}$ is an Hermitian matrix that can be determined entirely from the ideal-MHD o.d.e.s, (47) and (48), subject to physical boundary conditions at small and large r [6, 8]. Moreover, the real quantity E_{kk} can be interpreted as the *tearing stability index* [9] of a tearing mode that only reconnects magnetic flux at the kth rational surface.

4.5 Resistive Layers

In reality, the shielding current that flows in the vicinity of the kth rational surface does so in a thin resistive layer whose thickness (in r), δ_k, is much less than r_k [9]. We can define the complex dimensionless *layer response index*,

$$\Delta_k = \frac{\Delta\Psi_k}{\Psi_k}, \tag{59}$$

which characterizes the tearing parity response of the plasma in the layer to the tearing perturbation external to the layer. In general, Δ_k is a function of the (complex) frequency, ω, of the tearing mode, and is entirely determined by the layer. Equations (58) and (59) can be combined to give

$$\sum_{k'} (\Delta_k\, \delta_{kk'} - E_{kk'})\, \Psi_k, \tag{60}$$

where $\delta_{kk'}$ is a Kronecker delta symbol. The previous equation is the ultimate form of the tearing mode dispersion relation.

Note that the derivation of Eq. (60) depends crucially on the principle of *asymptotic matching*. According to this principle, the tearing perturbation is governed by the equations of perturbed, linearized, ideal-MHD throughout most of the plasma. However, these equations become singular at the various rational surfaces in the plasma. [See Eqs. (47) and (48).] The singularities are resolved by asymptotically matching the ideal-MHD solution to resistive layer solutions at each rational surface in the plasma. However, this procedure is only valid as long as the thicknesses of the resistive layers are less than the distances between successive rational surfaces. Let us investigate whether this is the case close to the magnetic separatrix.

5 Behavior Close to Magnetic Separatrix

5.1 Introduction

The aim of this section is to investigate asymptotic matching in the vicinity of the magnetic separatrix.

5.2 Spacing Between Successive Rational Surfaces

Suppose that $r_{k+1} > r_k$ for all values of k. In other words, suppose that the rational surfaces are indexed in order of increasing minor radius. In the vicinity of the magnetic separatrix, Eqs. (32) and (33) yield

$$\hat{r}_k \simeq \left[1 - \exp\left(-\frac{m_k}{n\,\alpha_-}\right)\right]^{1/2}. \tag{61}$$

for $\hat{r}_k < 1$, and

$$\hat{r}_k = \left[1 + \exp\left(-\frac{m_k}{n\,\alpha_+}\right)\right]^{1/2}. \tag{62}$$

for $\hat{r}_k > 1$. Here, $\hat{r}_k = r_k/a$.

The spacing (in $\hat{r}$) between successive rational surfaces is

$$\hat{\epsilon}_k(\hat{r}_k) = \frac{d\hat{r}_k}{dm_k} \tag{63}$$

for $\hat{r}_k < 1$, and

$$\hat{\epsilon}_k(\hat{r}_k) = -\frac{d\hat{r}_k}{dm_k} \tag{64}$$

for $\hat{r}_k > 1$. Thus,

$$\hat{\epsilon}_k(\hat{r}_k) = \frac{1 - \hat{r}_k^{\,2}}{2\,n\,\alpha_-\,\hat{r}_k}. \tag{65}$$

for $\hat{r}_k < 1$, and

$$\hat{\epsilon}_k(\hat{r}_k) = \frac{\hat{r}_k^{\,2} - 1}{2\,n\,\alpha_+\,\hat{r}_k}. \tag{66}$$

for $\hat{r_k} > 0$.

In the continuum limit, assuming that $\hat{r}_k \simeq 1$, the spacing between successive rational surfaces (in $\hat{r}$) becomes

$$\hat{\epsilon}(y) = \frac{|y|}{n\,\alpha}, \tag{67}$$

where $y = \hat{r} - 1$. Here, $\alpha = \alpha_-$ for $\hat{r} < 1$, and $\alpha = \alpha_+$ for $\hat{r} > 1$.

5.3 Magnetic Shear

In the vicinity of the magnetic separatrix, the magnetic shear can be written

$$s(\hat{r}) \equiv \frac{\hat{r}}{q}\frac{dq}{d\hat{r}} \simeq -\frac{1}{-y\,\ln(2\,|y|)}. \tag{68}$$

Note that the magnitude of the shear becomes infinite as the magnetic separatrix ($y = 0$) is approached.

5.4 Resistive Layer Quantities

It is helpful to define the following quantities that parameterize a resistive layer [11]:

$$\Lambda = 24 - \ln\left[\left(\frac{n_e}{10^6}\right)^{1/2}\left(\frac{e}{T_e}\right)\right], \tag{69}$$

$$\tau_{ei} = \frac{6\sqrt{2}\,\pi^{3/2}\,\epsilon_0^2\,m_e^{1/2}\,T_e^{3/2}}{Z\,\ln\Lambda\,e^4\,n_e}, \tag{70}$$

$$\eta_\parallel = \frac{m_e}{1.96\,n_e\,e^2\,\tau_{ei}}, \tag{71}$$

$$\tau_R = \frac{\mu_0\,r^2}{\eta_\parallel}, \tag{72}$$

$$\tau_A = \frac{R_0\,\sqrt{\mu_0\,m_i\,n_e}}{B_0}, \tag{73}$$

$$\tau_\perp = \frac{r^2}{\chi_\perp}, \tag{74}$$

$$\tau_\phi = \frac{r^2}{\chi_\varphi}, \tag{75}$$

$$d_\beta = \frac{\sqrt{(5/3)\,m_i\,(T_e + T_i)}}{e\,B_0}, \tag{76}$$

$$S = \frac{\tau_R}{\tau_A}. \tag{77}$$

Here, Z is the effective ion charge number, $T_e(r)$ is the electron temperature, $T_i(r)$ the ion temperature, m_i the ion mass, m_e the electron mass, $\chi_\perp(r)$ the perpendicular energy diffusivity, and $\chi_\phi(r)$ the perpendicular momentum diffusivity. Furthermore, $\tau_R(r)$ is the resistive diffusion time, $\tau_A(r)$ the Alfvén time, $\tau_\perp(r)$ the energy confinement time, $\tau_\phi(r)$ the momentum confinement time, $d_\beta(r)$ the ion sound radius, and $S(r)$ the Lundqvist number.

5.5 Resistive Layer Equation

Let $Y(r)\,\exp[\mathrm{i}\,(m\,\theta - n\,\phi - \omega\,t)]$ be the perturbed electron fluid stream-function. Consider the resistive layer centered on the kth rational surface. Let $X = S^{\,1/3}\,(r - r_k)/r_k$, where S is evaluated at radius r_k. We can write

$$\overline{Y}(p) = \int_{-\infty}^{\infty} Y(X)\,\mathrm{e}^{-\mathrm{i}\,p\,X}\,dX. \tag{78}$$

The boundary conditions are that $Y(p) \rightarrow 0$ as $p \rightarrow \infty$, and

$$Y(p) = Y_0\left[\frac{S^{-1/3}\,\Delta_k}{\pi\,p} + 1 + \mathcal{O}(p)\right] \tag{79}$$

at small values of p [11]. Here, Y_0 is an arbitrary constant, and Δ_k is the complex (dimensionless) layer response index introduced in Eq. (59).

Suppose that the layer physics is controlled by the three-field extended-MHD model described in Ref. [11]. In this case, the Fourier transformed layer equations reduce to the following equation:

$$\frac{d}{dp}\left[A(p)\,\frac{dY_e}{dp}\right]-\frac{B(p)}{C(p)}\,p^2\,Y_e=0, \tag{80}$$

where

$$A=\frac{(n\,s)^2\,p^2}{-\mathrm{i}\,(Q-Q_E-Q_e)+p^2}, \tag{81}$$

$$B=-\mathrm{i}\,(Q-Q_E)\,(Q-Q_E-Q_i)-\mathrm{i}\,(Q-Q_E-Q_i)\,(P_\varphi+P_\perp)\,p^2+P_\varphi\,P_\perp\,p^4, \tag{82}$$

$$C=-\mathrm{i}\,(Q-Q_E-Q_e)+[P_\perp-\mathrm{i}\,(Q-Q_E-Q_i)\,D^2]\,p^2+(1+1/\tau)\,P_\varphi\,D^2\,p^4. \tag{83}$$

Here,

$$Q=S^{1/3}\,\omega\,\tau_A, \tag{84}$$

$$Q_E=-S^{1/3}\,n\,\omega_E\,\tau_A, \tag{85}$$

$$Q_{e,i}=-S^{1/3}\,n\,\omega_{*\,e,i}\,\tau_A, \tag{86}$$

$$D=S^{1/3}\left(\frac{\tau}{1+\tau}\right)^{1/2}\hat{d}_\beta, \tag{87}$$

$$P_\perp=\frac{\tau_R}{\tau_\perp}, \tag{88}$$

$$P_\phi=\frac{\tau_R}{\tau_\phi}, \tag{89}$$

and

$$\omega_{*\,i}=-\frac{1}{e\,n_e}\,\frac{dp_i}{d\psi_p} \tag{90}$$

is the *ion diamagnetic frequency*. Here, $\hat{d}_\beta=d_\beta/r$. As before, all quantities are evaluated at radius r_k.

5.6 Solution of Resistive Layer Equation

As we saw in Sect. 5.3, the magnetic shear becomes very large as the magnetic separatrix is approached. If we treat $(n\,s)^2$ as much larger than the other parameters (e.g., Q, Q_e, $P_\perp$) that appear in Eqs. (80)–(83) then it is clear that the first term on the left-hand side of Eq. (80) dominates the second term for $p\lesssim 1$. In this case, we can solve the equation to give

$$Y(p)=Y_0\left\{\frac{S^{-1/3}\,\Delta_k}{\pi}\left[\frac{1}{p}+\frac{p}{\mathrm{i}\,(Q-Q_E-Q_e)}\right]+1+\mathcal{O}(p^2)\right\} \tag{91}$$

for $p\lesssim 1$, where use has been made of Eq. (79). Incidentally, the previous equation bears the hallmark of a *constant-ψ* layer response regime [9, 11].

Let $p=(n\,|s|)^{1/2}\,\hat{p}$. For $\hat{p}\gtrsim 1$, Eqs. (80)–(83) yield

$$\frac{d^2Y}{d\hat{p}^2}-\frac{B}{C}\,\hat{p}^2\,Y\simeq 0, \tag{92}$$

where

$$\begin{aligned}B&=-\mathrm{i}\,(Q-Q_E)\,(Q-Q_E-Q_i)-\mathrm{i}\,(Q-Q_E-Q_i)\,(P_\varphi+P_\perp)\,(n\,|s|)\,\hat{p}^2+P_\varphi\,P_\perp\,(n\,|s|)^2\,\hat{p}^4\\&\simeq P_\varphi\,P_\perp\,(n\,|s|)^2\,\hat{p}^4,\end{aligned} \tag{93}$$

$$\begin{aligned}C&=-\mathrm{i}\,(Q-Q_E-Q_e)+[P_\perp-\mathrm{i}\,(Q-Q_E-Q_i)\,D^2]\,(n\,|s|)\,\hat{p}^2+(1+1/\tau)\,P_\varphi\,D^2\,(n\,|s|)^2\,\hat{p}^4\\&\simeq(1+1/\tau)\,P_\varphi\,D^2\,(n\,|s|)^2\,\hat{p}^4,\end{aligned} \tag{94}$$

which reduces to

$$\frac{d^2Y}{dp^2}-G\,p^2\,Y\simeq 0, \tag{95}$$

where

$$G = \frac{P_\perp}{(1+1/\tau)\, D^2\, n^2\, |s|^2} = \frac{\tau_A^{2/3}\, \tau_R^{1/3}}{\tau_\perp\, \hat{d}_\beta^{\,2}\, (n\,|s|)^2}. \tag{96}$$

In the language of Ref. [11], we have a layer solution characterized by $k = 2$ and $\nu = 1/4$. It follows from Ref. [11] that

$$S^{-1/3}\, \Delta_k = \frac{\nu^{\,2\nu-1} \pi\, \Gamma(1-\nu)}{\Gamma(\nu)}\, [-\mathrm{i}\,(Q - Q_E - Q_e)]\, G^{\,\nu}, \tag{97}$$

where $\Gamma(z)$ is a gamma function [12]. Hence, in the continuum limit,

$$\Delta = \frac{2\pi\, \Gamma(3/4)}{\Gamma(1/4)}\, (-\mathrm{i})\, [\omega + n\,(\omega_E + \omega_{*\,e})]\, \frac{\tau_A^{1/2}\, \tau_R^{3/4}}{\tau_\perp^{1/4}\, \hat{d}_\beta^{\,1/2}\, (n\,|s|)^{1/2}}, \tag{98}$$

where all terms on the right-hand side are evaluated at radius r. Thus, we deduce that the strong magnetic shear in the vicinity of the magnetic separatrix forces all of the resonant layers in this region to lie in the so-called *diffusive-resistive* regime introduced in Ref. [11].

The thickness of the a given layer in p-space is $|G|^{-\nu}$ [11], so the thickness in $\hat{r}$ space is

$$\hat{\delta} = \frac{\tau_A^{1/2}}{\tau_R^{1/4}\, \tau_\perp^{1/4}\, \hat{d}_\beta^{\,1/2}\, (n\,|s|)^{1/2}}. \tag{99}$$

Funding
This research was funded by the U.S. Department of Energy, Office of Science, Office of Fusion Energy Sciences under contract DE-FG02-04ER54742.

Acknowledgments

Data availability
The digital data used in the figures in this paper can be obtained from the author upon reasonable request.

References

[1] J.A. Wesson, *Tokamaks*, 4th edition. (Oxford University Press, Oxford UK, 2011).

[2] A.H. Boozer, Rev. Mod. Phys. **76**, 1071 (2004).

[3] R. Fitzpatrick, Nucl. Fusion **33**, 1049 (1993).

[4] N. Pomphrey and A. Reiman, Phys. Fluids B **4**, 938 (1992).

[5] R.D. Hazeltine and J.D. Meiss, Phys. Reports, **121**, 1 (1984).

[6] R. Fitzpatrick, R.J. Hastie, T.J. Martin and C.M. Roach, Nucl. Fusion **33**, 1533 (1993).

[7] M. Abramowitz and I.A. Stegun, *Handbook of Mathematical Functions*, (Dover, New York NY, 1964), chap. 5.

[8] R. Fitzpatrick, Phys. Plasmas **31**, 102507 (2024).

[9] H.P. Furth, J. Killeen and M.N. Rosenbluth, Phys. Fluids **6**, 459 (1963).

[10] C. Mercier, Nucl. Fusion **1**, 47 (1960).

[11] R. Fitzpatrick, Phys. Plasmas **29**, 032507 (2022).

[12] M. Abramowitz and I.A. Stegun, *Handbook of Mathematical Functions*, (Dover, New York NY, 1964), chap. 6.